Available online at www.sciencedirect.com

SciVerse ScienceDirect

Journal of the European Ceramic Society 32 (2012) 2469–2476

www.elsevier.com/locate/jeurceramsoc

Co-precipitation of a Ni–Zn ferrite precursor powder: Effects of heat treatment conditions and deagglomeration on the structure and magnetic properties

Susana M. Olhero [a,b,*], Das Soma [d], Vitor S. Amaral [d], Tim W. Button [b], Fernando J. Alves [a], José M.F. Ferreira [c]

[a] Department of Mechanical Engineering, FEUP, University of Porto, Porto, Portugal
[b] IRC in Materials Processing, School of Metallurgy and Materials, University of Birmingham, Birmingham B15 2TT, UK
[c] Department of Ceramic and Glass Engineering, CICECO, University of Aveiro, 3810-193 Aveiro, Portugal
[d] Department of Physics and CICECO, University of Aveiro, 3810-193 Aveiro, Portugal

Received 3 January 2012; received in revised form 7 March 2012; accepted 9 March 2012
Available online 10 April 2012

Abstract

A Ni–Zn ferrite precursor powder was synthesized by co-precipitation upon adding ammonia to an aqueous solution of the precursor iron, nickel, and zinc nitrate salts. The powder was calcined at a range of temperatures (200–1200 °C) and the crystalline phase evolution was assessed by X-ray diffraction coupled with Rietveld refinement. Intermediate phases ($NiFe_2O_4$ and Fe_2O_3) with increasing crystallinity coexisted in the system up to 1000 °C. The required $Ni_{0.8}Zn_{0.2}Fe_2O_4$ phase could only be attained at 1200 °C. The magnetic properties measured using a vibrating sample magnetometer revealed high magnetization saturation level (∼59 emu/gm) above 400 °C. The coercivity showed a steady decrease with increasing heat treatment temperature, leading to a change from a hard to soft magnetic state. The BET specific surface area and the SEM morphology were found to be dependent on calcination temperature, atmosphere (air or N_2) and on the milling procedure.

Keywords: Magnetic materials; Chemical syntheses; Ni–Zn ferrites; Surface properties; Rietveld refinement

1. Introduction

Ni–Zn ferrite with the spinel structure is a versatile technological material due to its high-resistivity and low-Eddy current losses, and is particularly suitable for high-frequency applications. Ni–Zn ferrites have been commercially used in applications including recording heads, antenna rods, loading coils, microwave devices and the telecommunication field.[1,2] In the typical ion configuration for Ni–Zn bulk ferrites (for low Zn concentration), Ni and Zn ions occupy B-site and A-site positions respectively. The incorporation of divalent zinc into the A-site leads to a substantial increase of the magnetization in the ferrimagnetic state, from 2.34 μ_B per formula unit in pure Ni ferrite to 3.65 μ_B per formula unit in 20% substituted Zn ferrite.[3]

The microstructure and magnetic properties of Ni–Zn ferrites are highly sensitive to composition, sintering conditions, grain size, the nature and amount of any additives and impurities and the preparation methodology. Therefore, the chemical composition and processing methods are critical factors that determine the physical properties of ferrites. Recently, many publications have reported various "bottom up" preparation techniques based on wet-chemical reactions to obtain ferrite powders. The most popular are: sol–gel methods,[4–6] microemulsion[7] hydrothermal-microwave[8] and hydrothermal synthesis,[9–11] and co-precipitation.[12–14] The wet chemical synthesis of highly reactive powders has proved to be one of the most effective routes to decrease the reaction temperature to obtain ferrites. Co-precipitation and sol–gel methods produce homogeneous, fine and reproducible precursor ferrite powders, i.e., metal oxides are

* Corresponding author at: Department of Mechanical Engineering, FEUP, University of Porto, Porto, Portugal. Tel.: +351 234 370261; fax: +351 234 370204.
E-mail address: susana.olhero@ua.pt (S.M. Olhero).

0955-2219/$ – see front matter © 2012 Elsevier Ltd. All rights reserved.
doi:10.1016/j.jeurceramsoc.2012.03.017

firstly obtained by chemical synthesis without ferrite formation and, subsequently, high temperatures are needed to promote their chemical reaction to form different kinds of ferrites.[10,12,15] From the thermal dynamics viewpoint, it is well established that densification is enhanced by using fine-grained powders exhibiting high surface free energy. However, increased diffusion activity on strongly curved surfaces is a feature of an individual particle only, whereas the densification activity describes the interaction of a multitude of particles, and the high surface of particles is also a strong driving force for agglomeration. The formation of agglomerates resulting in inhomogeneous pore size distribution may considerably retard densification and increase the average grain size of sintered bodies.[16]

The synthesis of ferrites by using "top-down" methods, such as high energy mechanical milling, has been also reported.[17–20] This means that besides deagglomerating the starting component precursor powders, the milling energy might also induce the formation of new crystalline phases and change the surface characteristics of the ferrite powders. The effects of morphological/chemical changes occurring during milling on the dispersion ability of ferrite powders have not been reported so far. Thus, the present study aims at synthesising Ni–Zn ferrite particles in two steps: chemical co-precipitation of corresponding precursor oxides and their chemical reaction at high temperature. The precursor powder mixture heat treated at 400 °C was selected to evaluate the effects of other physical treatments (milling/atmosphere of heat treatment) on the crystalline phase assembly, the physical characteristics of the powders, including the magnetic properties. This temperature (400 °C) represented a good compromise between incipient magnetic properties and a low degree of powder agglomeration.

2. Experimental procedure

The synthesis of the ferrite precursor powder was performed by the co-precipitation method using high-purity nickel nitrate hexahydrate [$Ni(NO_3)_2{\bullet}6H_2O$, Sigma Aldrich, Germany], zinc nitrate hexahydrate [$Zn(NO_3)_2.6H_2O$, Sigma Aldrich, Germany] and iron nitrate nonahydrate [$Fe(NO_3)_3{\bullet}9H_2O$, Sigma Aldrich, Germany] as starting materials. Ammonia solution (ammonium hydroxide solution, ca 25% NH_3, Sigma Aldrich, Germany) was also used as precipitating agent. The cationic reagents corresponding to 0.25 mol of $Ni_{0.8}Zn_{0.2}Fe_2O_4$ ferrite were weighted separately, dissolved in a beaker containing about 0.9 L of de-ionized water and then transferred to a volumetric borosilicate glass flask, adding the necessary water to complete the total volume of 1 L. This cationic solution was heated to 80 °C under continuous mechanical stirring, and then ammonia solution was slowly added to set the pH at around 9.5. The synthesis conditions (temperature, pH and mechanical stirring) were kept constant for 2 h in order to complete the reaction. The precipitated powder was filtered and washed twice with distilled water and then dried at 80 °C for 48 h.

The thermal behaviour of the dried powder from room temperature up to 1200 °C was assessed by DTA/TG analysis (SETARAM, Labsys, Caluire, France) using a heating rate of 10 °C/min. Based on the results observed, powder samples were then calcined at 200, 300, 400, 600, 800, 1000 and 1200 °C for 1 h, to study the effects of heat treatment on crystalline phase evolution. Heat treatments were carried out in a Thermolab furnace with a heating rate of 5 °C/min to achieve the preset temperature, followed by a dwelling time of 1 h and then cooled to room temperature at the rate of 5 °C/min. A calcination temperature of 400 °C was then selected to study the effects of the heat treatment atmosphere and deagglomeration method of the powders on their properties. This temperature represented a good compromise between the incipient magnetic properties and a low degree of powder agglomeration. Accordingly, powder samples were treated as follows: (i) air atmosphere; (ii) air atmosphere + hand deagglomeration in a mortar; (iii) air atmosphere + planetary milling for 4 h in ethanol; and (iv) air atmosphere + planetary milling for 4 h in ethanol, followed by calcination in nitrogen atmosphere at 400 °C for 1 h; (v) the same as (iv) + hand deagglomeration in a mortar. Sample codes and the respective experimental conditions used are presented in Table 1.

Table 1
Samples' codes and respective post synthesis procedures for NiZn ferrite powders obtained by co-precipitation.

Sample code	Preparation conditions
Sample 1	NiZn ferrite calcined at 400 °C in air before milling
Sample 2	Sample 1 after deagglomeration in a mortar
Sample 3	Sample 1 planetary milled in ethanol
Sample 4	Sample 3 heat treated again at 400 °C but in N_2 atmosphere

Qualitative and quantitative analysis of crystalline phases in the resultant Ni–Zn ferrite powders were determined by X-ray diffraction (XRD) analysis using a conventional Bragg–Brentano diffractometer (Philips PW 3710, Eindhoven, Netherlands) with Ni-filtered Cu-K_α radiation. X-ray diffraction data were recorded in 2θ range = 5–100° (step size 0.02° and 6 s of counting time for each step). The phase fractions were extracted by Rietveld-RIR (reference intensity ratio) refinements, using GSAS software and EXPGUI. The background was successfully fitted with a Chebyshev function with a variable number of coefficients depending on its complexity. The peak profiles were modeled using a pseudo-Voigt function with one Gaussian and one Lorentzian coefficient. Lattice constants, phase fractions, and coefficients corresponding to sample displacement and asymmetry were also refined.

The specific surface area was determined by the nitrogen adsorption BET method using a Surface Area Analyzer (Gemini, Micromeritics, USA). Density and particle size distribution of the powders were measured by using helium gas picnometer (Accupyc Quantachrome, Florida, USA) and laser scattering analyser (Coulter LS 230, Buckinghamshire, UK), respectively. Scanning Electron Microscopy (SEM, Hitachi S-4100, Tokyo, Japan) was used to analyse the shape and state of agglomeration of Ni–Zn ferrite particles treated under different conditions. Magnetization measurements were made on a Vibrating Sample Magnetometer (VSM, Cryogenics, UK) at room temperature using a field up to 10 T.

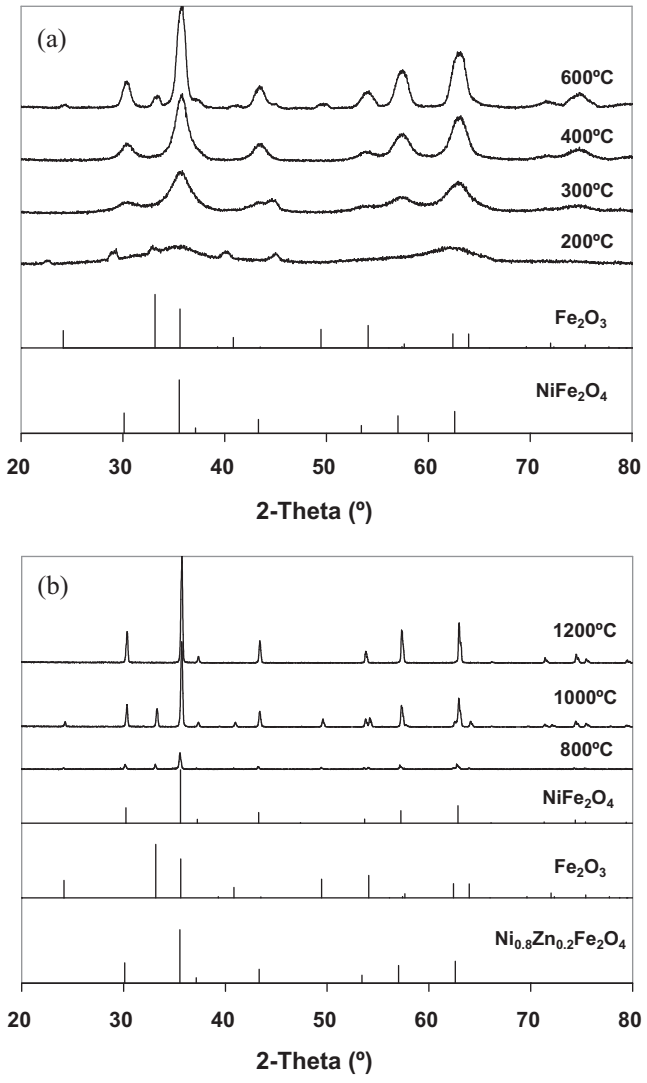

Fig. 1. XRD patterns of Ni–Zn ferrite powder calcined at different temperatures in the ranges of 200–600 °C (a); and of 800–1200 °C (b).

3. Results and discussion

3.1. Thermal behaviour of the precipitated precursor ferrite powder

The DTA/TG curves of the precipitated powder after being dried at 80 °C (not shown) revealed an almost linear weight loss rate from approximately the drying temperature (80 °C) to about 240 °C, which can be attributed to the gradual dehydration of the precipitated species (likely amorphous hydroxides). Then, a sudden weight loss accompanied by a strong exothermic effect occurred at around 250 °C. Such exothermic effect can hardly be attributed to the transformation from amorphous to crystalline matter. In fact, Fig. 1a reveals that the degree of crystallinity changed only slightly when the heat treatment temperature increased from 200 to 300 °C. This strong exothermic effect can be attributed do the decomposition of residual ammonium nitrate according to the reaction (1)[21,22]:

$$NH_4NO_3 \rightarrow 2\,N_{2(g)} + 2H_2O_{(l)} + O_{2(g)} \quad (1)$$

Table 2
Surface area (BET) and D_{50} of the NiZn ferrite powders calcined at different temperatures from 300 to 1200 °C.

Calcination temperature in air atmosphere (°C)	Specific surface area (m^2/g)	D_{50} (μm)	Density (g/dm^3)
200	149.07	22.96	2.417 ± 0.05
300	99.57	26.88	5.132 ± 0.184
400 (Sample 1)	76.82	29.48	5.351 ± 0.107
600	13.13	46.75	5.345 ± 0.162
800	0.251	75.22	5.349 ± 0.251
1000	0.111	191.5	5.360 ± 0.051
1200	0.078	258.2	5.365 ± 0.020

The explosive properties of ammonium nitrate are well known, which become much more evident at elevated temperatures.[21,22]

After the sudden decomposition of ammonium nitrate remains, the TG curve retook approximately the same slope as before, suggesting that the dehydration process continued at about the same rate, becoming almost complete up to 400 °C. Practically, no further weight changes could be registered beyond 500 °C.

The XRD patterns of Ni–Zn ferrite powders calcined for 1 h in air atmosphere at temperatures from 200 °C to 600 °C and from 800 °C to 1200 °C are shown in Fig. 1a and b, respectively. Broad peaks of intermediate phases ($NiFe_2O_4$ and Fe_2O_3) could be identified at 200 °C, becoming gradually sharper as the heat treatment temperature was increased. The peak broadening observed for the samples treated at the lower temperatures reflects the ultra-fine nature of the crystallites and the presence of amorphous material. The required phase, $Ni_{0.8}Zn_{0.2}Fe_2O_4$, could only be attained at 1200 °C, indicating that the free hematite existing at lower temperatures gradually reacted during sintering, particularly for $T \geq 1000$ °C. The complete transformation into Ni–Zn ferrite phase at 1200 °C is consistent with the results obtained by other authors.[23]

Density and average particle/agglomerate size (D_{50}) data of the Ni–Zn ferrite powders calcined at different temperatures in air atmosphere are presented in Table 2. As expected, D_{50} increases as the heat temperature increases, a reflection of an increasing agglomeration trend. The powder calcined at 200 °C presents a much lower (less than half) density in comparison to the theoretical density of Ni–Zn ferrite and other phases present ($NiFe_2O_4 = 5.372$ g/cm^3, $Fe_2O_3 = 5.267$ g/cm^3 and $Ni_{0.8}Zn_{0.2}Fe_2O_4 = 5.324$ g/cm^3). This can be attributed to its high hydrated state as could be deduced from the results of thermal analysis. The density of the sample calcined at 400 °C reaches a value similar to that of Ni–Zn ferrite, which then remained almost constant with further increasing the heat treatment temperature.

Performing quantitative XRD analysis of the crystalline phases in this system is tricky because the diffraction peaks of the expected Ni–Zn ferrite phase ($Ni_{0.8}Zn_{0.2}Fe_2O_4$) are approximately coincident with those of $NiFe_2O_4$ and Ni–Zn ferrites with other Ni/Zn ratios. This applies particularly to the spectra obtained at lower calcination temperatures that include broad peaks. This dilemma has been also reported by other authors who

Table 3
Results of Rietveld RIR quantitative analysis (wt.%) for Ni–Zn ferrite powder calcined at temperatures from 300 to 1200 °C.

Calcination temperature (°C)	$NiFe_2O_4/ZnFe_2O_4$ (wt.%)	Fe_2O_3 (wt.%)	$Ni_{0.8}Zn_{0.2}Fe_2O_4$ (wt.%)	Total	χ^2	R_{wp}	R_p	$a(NiFe_2O_4)$ (Å)	$a = b$ (Fe_2O_3) (Å)	$a(NiZnFe_2O_4)$ (Å)	$c(Fe_2O_3)$ (Å)
300	91.4(1)	8.59(1)	–	100	1.145	0.0216	0.0170	8.3909	5.1445		12.4649
400 (Sample 1)	90.8(0)	9.20(1)	–	100	1.134	0.0132	0.0105	8.3644	5.0685		12.9202
600	88.3(3)	11.7(5)	–	100	1.122	0.0212	0.0168	8.3491	5.0271		13.7274
800	72.2(8)	27.8(4)	–	100	1.245	0.0228	0.0180	8.3480	5.0287		13.7190
1000	73.1(1)	26.9(5)	–	100	1.957	0.0175	0.0129	8.3474	5.0293		13.7144
1200/1 h	69.7(1)	–	30.3 (5)	100	1.700	0.0257	0.0190	8.3431	–	8.3461	–
1200/4 h	18.1(4)	–	81.9 (6)	100	4.108	0.0145	0.0091	8.3449	–	8.3609	–

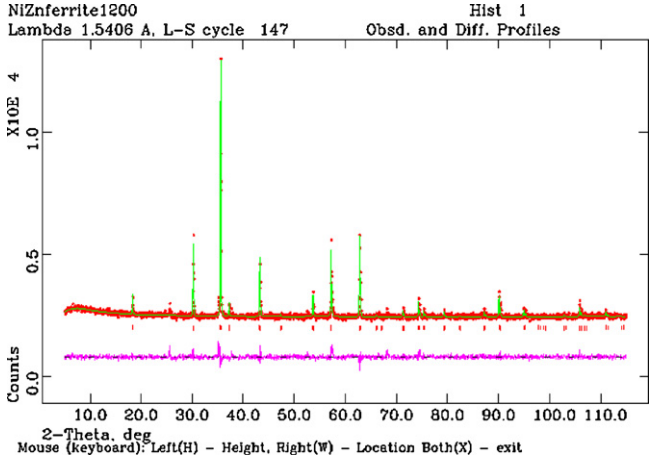

Fig. 2. Observed (crosses), calculated (continuous line), and difference curve from the Rietveld refinement of the Ni–Zn ferrite calcined at 1200 °C.

observed a shift of X-ray reflections towards small angles with increasing zinc content.[24] The authors attributed this behaviour to the increase in the crystallographic cell dimensions with increasing zinc content. However, this 2-theta shifting can only be observed if sharper peaks are present. Therefore, Rietveld refinement was used in the present work as a tool to assess the qualitative and quantitative information about the crystalline phases formed as a function of the heat treatment temperature. Table 3 presents the quantitative analysis of the crystalline phases present in all the samples calcined at different temperatures as obtained from XRD analysis combined with the Rietveld RIR technique. Fig. 2 shows the fit of a measured XRD pattern of the Ni–Zn ferrite calcined at 1200 °C by using the GSAS EXPGUI software.

The calculated diagram (Fig. 2) is based on crystallographic structure models, which also take into account specific instrument and sample effects. The parameters of this model have been refined simultaneously using least-squares methods in order to obtain the best fit to all measured data. By least squares refinement, a so-called figure-of-merit function R has been defined, which describes the residual (agreement) between observed and calculated data. It is noteworthy that many different statistical R factors have been proposed for judging the quality of a Rietveld refinement. The R factors show the mean deviation from the model in per cent. The "profile R-factor", R_p, and "weighted profile R-factor", R_{wp}, for all the refinements are presented in Table 3. The values of R_{wp} as obtained in the present investigation are well within the limits of experimental accuracy. The difference plot in Fig. 2 does not show any significant misfits. As is evident from Table 3, the crystalline phase, $Ni_{0.8}Zn_{0.2}Fe_2O_4$, is only formed after calcination at 1200 °C, and even then is mixed with $NiFe_2O_4$. Increasing the reaction time from 1 h to 4 h at this temperature (1200 °C) further promoted the thermal reaction and resulted in a significant increase of the amount of $Ni_{0.8}Zn_{0.2}Fe_2O_4$, as expected. $NiFe_2O_4$ and $ZnFe_2O_4$ were always present as the main crystalline phases, especially in the samples calcined at the lower temperatures, in which they reach together a crystalline fraction of ~90%. These two phases are not distinguishable from the

GSAS program since they present similar cell parameters and cell volumes, but a mixture of both is likely to be formed. Fe_2O_3 was also present as a secondary phase, the fraction of which increased up to 800–1000 °C, being accompanied by a concomitant decreasing amount of $NiFe_2O_4$/$ZnFe_2O_4$. The Fe_2O_3 phase then disappeared with the temperature further increasing.

It is important to mention that the accuracy of the phase analysis is less for heat treatment temperatures below 600 °C, because of the low crystallinity of the samples. Moreover, the fact that only about 82% of the planed ferrite composition has been achieved after sintering at 1200 °C for 4 h might be related to small deviations from stoichiometry due to partial evaporation of zinc and niquel in the form of ZnO and NiO. To ascertain this, we have determined the weight loss underwent by the precursor powder within the temperature range of 600–1200 °C. A total weight loss of 0.9% was found. Even assuming that all the mass lost was solely due to evaporation of ZnO, this would correspond to 12.15% loss of total ZnO in the system.

According to the XRD results, the material is mostly amorphous when calcined at low temperatures, becoming increasing crystalline as the heat treatment temperature is increased. The amount of the amorphous phase was only qualitatively deduced from the peak broadening effects. Quantitative phase analysis using the common internal standards tested (Al_2O_3 and LaB_6) could not be performed due to the close matching of XRD peaks of the standards and samples at the same 2-theta values. For calcination temperatures up to 1000 °C the $NiFe_2O_4$/$ZnFe_2O_4$ and Fe_2O_3 phases coexisted with some amorphous material, and Rietveld analysis did not show any relevant local deformation in these phases at the atomic level, as the relative changes in their lattice parameters were limited to ~1%. Average crystallite sizes of the calcined samples have been calculated from XRD diffraction peaks and increase gradually from 1.5 nm at 200 °C to 8.6 nm at 600 °C. A substantial increase to 39.3 nm occurred upon heat treating at 800 °C, followed by a further increase to 43.4 nm up to 1200 °C.

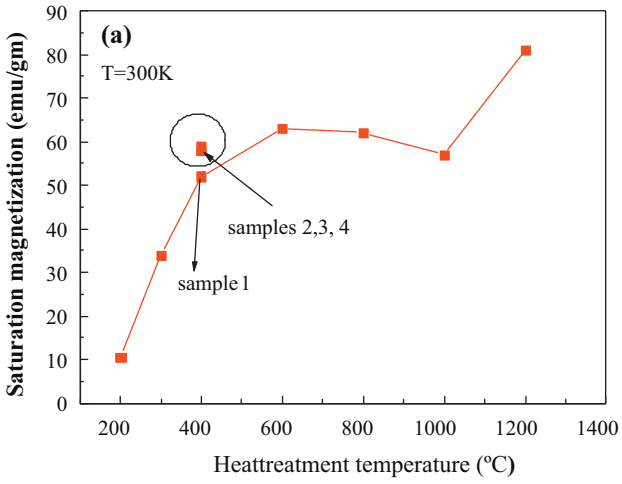

Fig. 3. Variation of saturation magnetization of (NiZn)Fe_2O_4 with calcination temperature (particle size).

The effect of heat treatment temperature on magnetic properties was investigated through isothermal magnetization at room temperature (300 K) up to an external field of 10 T (Fig. 3). Samples calcined in the temperature range of 200–600 °C show a steady increase of magnetization with magnetic field, without

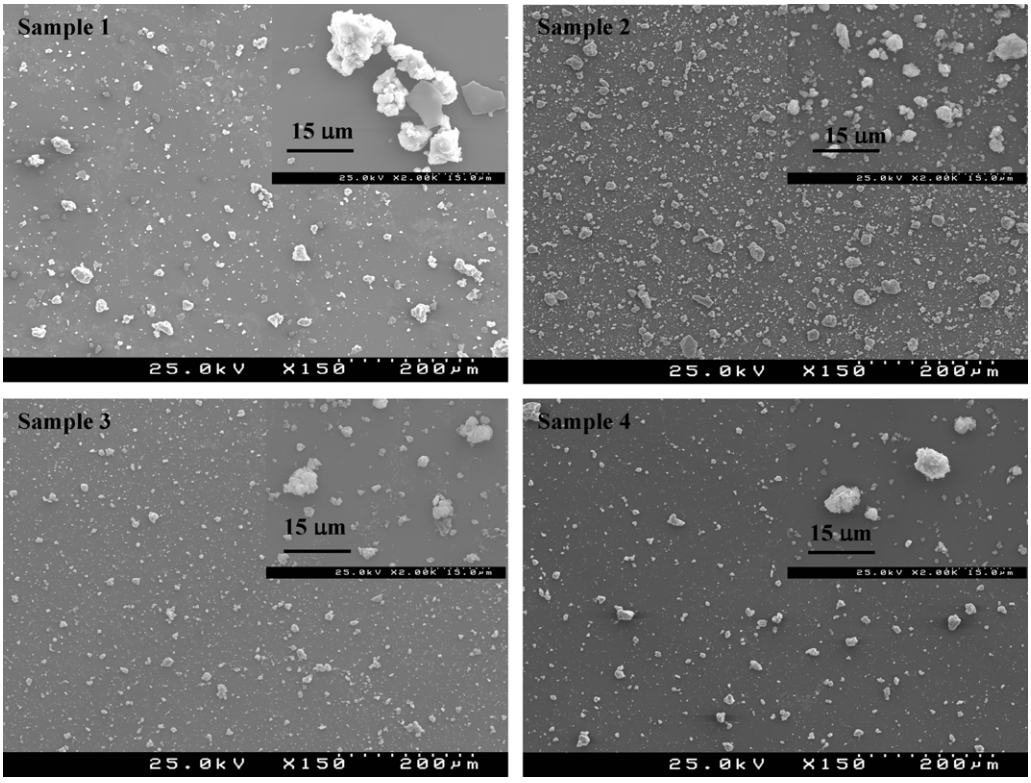

Fig. 4. SEM micrographs of the NiZn ferrite powders calcined at 400 °C in environment and nitrogen atmosphere and milled in different conditions.

reaching saturation even at 10 T. A clear saturation at low fields (in the range above 0.5 T) is only observed in samples calcined at or above 800 °C. The magnetization at maximum field increased with calcination temperature reaching values of ∼50–60 emu/g (2.1–2.5 μ_B per formula unit), with small variations in the range of 400–1000 °C. A detailed analysis reveals that the magnetization field is higher for the sample calcined at 600 °C with a slight decreasing trend with further increasing the calcination temperature up to 1000 °C. Finally, a large increase in the saturation magnetization to ∼80 emu/g (3.4 μ_B per formula unit), was registered for the sample calcined at 1200 °C. These changes can be understood relating to the progressive phase modifications and crystallite average sizes with increasing calcination temperature. The initial increase of magnetization value reflects mostly the reduction of structural disorder and grain/crystallite growth, stepping when values reach the Ni ferrite value (2.3 μ_B per formula unit) at calcination temperature 600 °C. The further slight decreasing trend correlates well with an apparent increase of the amount of antiferromagnetic Fe_2O_3 phase (Table 3). Finally, the sudden jump in the magnetization to ∼80 emu/g confirms that only at 1200 °C the required crystalline phase, $Ni_{0.8}Zn_{0.2}Fe_2O_4$ (with expected 3.65 μ_B per formula unit) is formed and dominates, but still containing some amount of Ni ferrite phase. Moreover, the absence of clear saturation at lower applied fields below 800 °C calcination temperature correlates with the smaller crystallite size below 10 nm, which leads to a substantial surface to volume ratio with inherent surface magnetization disorder and frustrated magnetic interactions.

A more quantitative analysis of results is made difficult from the interplay of phase composition modifications and crystallinity effects, particularly at intermediate temperatures. At 400 °C the magnetization may be masked by the amount of amorphous phase, while within the temperature range 600–1000 °C it might be affected by the increasing amounts of antiferromagnetic Fe_2O_3 in the system. As a result, the measured coercive field does not present a clear trend with calcination temperature, remaining in the range 0.009–0.0250 T (90–250 Oe), the lowest value being obtained in the sample calcined at 1200 °C, correlating also with the formation of Ni–Zn ferrite. The expected values for Ni ferrite and Ni–Zn ferrite are 0.019 and 0.005 T, respectively. The highest value is found in the sample calcined at 600 °C. For a pure material, due to change in effective anisotropy, one might expect an initial increase with crystallite size and a further decrease as the multi-domain region is reached.[25]

3.2. *Effects of heat treatment atmosphere and of deagglomeration procedure*

The quality of ceramic processing strongly depends on the powders, namely, on particle/agglomerate size and particle/agglomerate size distribution, specific surface area, etc. These characteristics, in turn, are dependent on the thermal history and eventually, on the heat treatment atmosphere. Based on these considerations and on the results presented above, the temperature of 400 °C was selected to study the effects of heat treatment atmosphere and of deagglomeration procedure on the magnetic and surface properties of the particles.

Table 4
Results of Rietveld RIR quantitative analysis (wt.%) for Ni–Zn ferrite powder calcined at 400 °C (O_2 or N_2) and subjected to different milling conditions.

Sample code (see Table 1)	Specific surface area (m^2/g)	D_{50} (μm)
1	76.82	29.48
2	85.82	5.120
3	131.83	1.505
4	99.57	2.454

Table 4 presents the specific surface area and average particle size data of the Ni–Zn ferrite powder calcined at 400 °C in air atmosphere (Sample 1) and subjected to different milling procedures (Samples 2 and 3) and to a further calcination step under nitrogen atmosphere (Sample 4) as reported in Table 1. From these data, it can be concluded that Sample 1 consists of coarse agglomerates with average diameter of about 30 μm, which are porous as can be deduced from the relatively high specific surface area (∼77 m^2/g). Deagglomeration decreases the average particle/agglomerate size and consequently increases specific surface area, as expected. It can also be deduced that wet milling in ethanol is more effective than dry milling in the mortar. A partial reagglomeration occurred upon further heat treating Sample 3 in a nitrogen atmosphere to obtain Sample 4. The changes reported in Table 4 are consistent with the morphological features of the different powders (Samples 1–4) presented in Fig. 4. Sample 3 is the finest one, followed by Sample 4.

Fig. 5 shows XRD patterns of the Ni–Zn ferrite powder calcined at 400 °C in air atmosphere (Sample 1) and submitted to different milling procedures (Samples 2 and 3) and to a further calcination step under nitrogen atmosphere (Sample 4) as reported in Table 1. Their quantitative analysis evaluated by Rietveld refinement (without considering the amorphous fraction) (Table 5) confirms that crystalline $NiFe_2O_4$ and Fe_2O_3 phases have been formed. Table 5 shows that deagglomerating the powder (irrespective of dry or wet milling) seems to change the apparent partition of $NiFe_2O_4$ and Fe_2O_3 phases from about 91% to about 95% of $NiFe_2O_4$. Considering the low energy

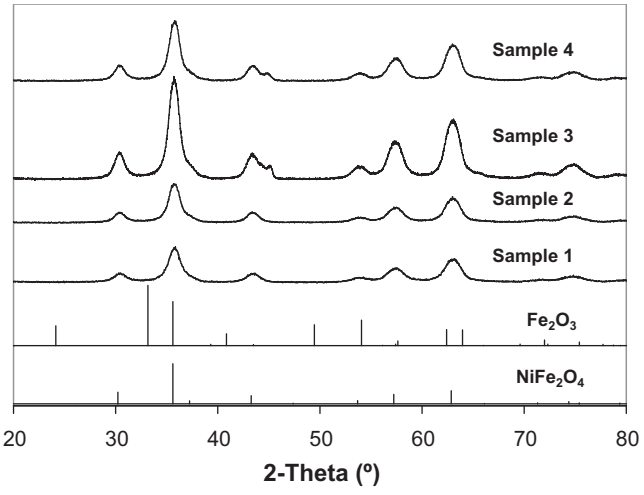

Fig. 5. XRD patterns of NiZn ferrite powder calcined at 400 °C (O_2 or N_2) and milled in different conditions.

Table 5
Surface area (BET) and D_{50} of the NiZn ferrite powders calcined at 400 °C in air and nitrogen atmosphere and milled under different conditions.

Sample code (see Table 1)	1	2	3	4
$NiFe_2O_4/ZnFe_2O_4$ (wt.%)	90.8 (0)	95.7 (0)	94.1 (0)	94.8 (3)
Fe_2O_3 (wt.%)	9.20 (1)	4.30 (1)	5.99 (3)	5.2 (4)
Total	100	100	100	100
χ^2	1.134	1.539	1.113	1.342
R_{wp}	0.0132	0.0116	0.0131	0.0144
R_p	0.0105	0.0090	0.0106	0.0113
$a(NiFe_2O_4)$ (Å)	8.3644	8.3574	8.3442	8.3502
$a(Fe_2O_3)$ (Å)	5.0685	5.0496	5.1169	5.0387
$c(Fe_2O_3)$ (Å)	12.9202	12.3674	12.8567	12.3306

features of both milling procedures used, these changes might be more apparent than real. This suggests that Sample 1 might consist of particles having a kind of core–shell structure and its XRD analysis reflects more preferentially the outer part composition. This hypothesis is supported by the XRD results presented in Fig. 6. These results reveal that the XRD peaks became sharper upon deagglomeration, with the difference being better noticed for the lower heat treatment temperatures. Such differences are probably induced by the contact with air atmosphere. As a matter of fact, heat treating the Sample 3 in nitrogen atmosphere to obtain Sample 4 did not change the crystalline phase composition, as can be seen in Table 5.

The present results show that the smallest particle sizes were obtained for the sample wet milled in ethanol followed by the one dry deagglomerated in a mortar. The higher efficacy of wet versus dry milling of solids has been already proved.[26] The enhanced effectiveness of wet milling was explained by the

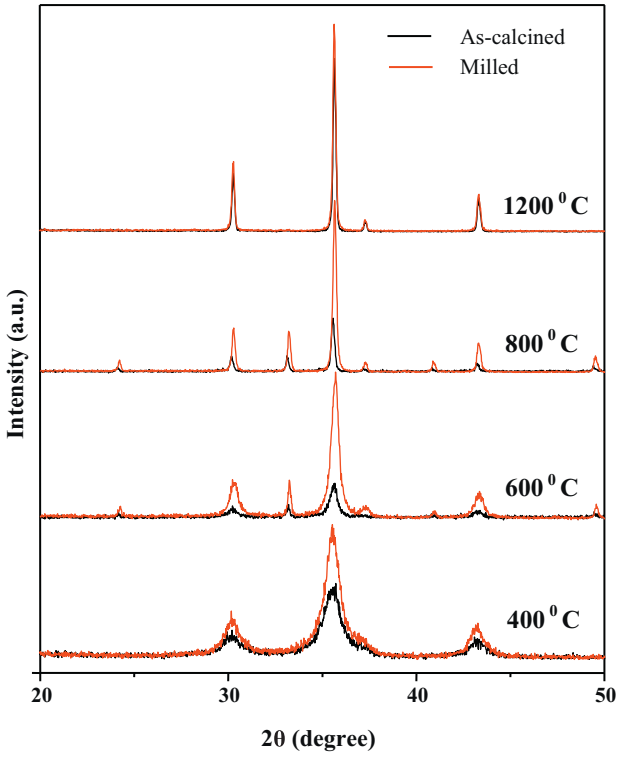

Fig. 6. XRD patterns of the ferrite powders calcined at different temperatures before and after hand milling in a mortar.

saturation of unsaturated bonds on the surface of the material by liquid molecules, with the liquid layers around the grains favouring the disintegration of the material.[27] The data reported in Table 4 together with the micrographs shown in Fig. 4 suggest that the specific surface area and morphological features of powders calcined at 400 °C are essentially dependent on the milling/deagglomeration procedure used and less on the heat treatment atmosphere.

The saturation magnetization data of the Samples 1–4 presented in Fig. 3, show that original sample has lowest magnetization due to the highest amount of Fe_2O_3, which then increases for about 16% upon milling (Samples 2 and 3) and further calcination under nitrogen atmosphere (Sample 4). These results suggest that the saturation magnetization is sensitive to the state of agglomeration of the powder (milling procedure) and also to the amount of Fe_2O_3 (Table 5). The average size, D_{50}, decreased from about 30 μm for Sample 1, to ~5 μm and ~1.5 μm for the Samples 2 and 3, respectively, upon deagglomerating the powder in a mortar or wet ball milling in ethanol. These values are much larger than crystallite sizes (which did not change appreciably with these procedures remaining within 6.1–6.9 nm), so they are not expected to have direct influence on the magnetization of the intrinsic materials. However, milling and further annealing might promote zinc incorporation in the ferrite, (even at low levels at the surface) leading to the observed increase of magnetization.[27]

4. Conclusions

Precursor Ni–Zn ferrite fine powders were easily synthesized by co-precipitation. The heat treatment conditions (temperature, atmosphere) and the method used to deagglomerate the calcined powders play important roles in determining the magnetic properties and the state of agglomeration. Crystallinity and magnetization were both enhanced by increasing calcination temperature. The required phase, $Ni_{0.8}Zn_{0.2}Fe_2O_4$, appeared only at 1200 °C, although other magnetic phases such as $NiFe_2O_4/ZnFe_2O_4$ together with the antiferromagnetic Fe_2O_3 were formed at temperatures between 300 °C and 1000 °C. At 400 °C magnetic $NiFe_2O_4/ZnFe_2O_4$ phases and Fe_2O_3 were identified but the amount of amorphous matter having a similar density as the magnetic phases seems to prevail.

The mild milling conditions used were not expected to influence the crystalline phase assemblage, although the apparent

phase fractions were different, probably due to the lack of homogenization in a kind of core–shell structure induced by the contact with air atmosphere. Moreover, wet milling is more efficient in reducing particle size than hand deagglomeration in a mortar. Using a nitrogen atmosphere has no significant variations in the amount of phases formed.

Acknowledgements

S.M. Olhero thanks to the Foundation for Science and Technology of Portugal (FCT) for the financial support under the grant SFRH/BPD/27013/2006. Soma Das acknowledges FCT for the grant SFRH/BPD/39262/2007. The authors would also like to thank CICECO for the work at the University of Aveiro and FCT for the financial support under the project PTDC/CTM/099489/2008.

References

1. Stoppels D. Developments in soft magnetic power ferrite. *Journal of Magnetism and Magnetic Materials* 1996;**160**(1):323–8.
2. Robert CO. *Modern magnetic materials principles and application*. Beijing: Industry of Chemistry Press; 2003.
3. Goldman A. *Modern ferrite technology*. 2nd ed. New York: Springer; 2006.
4. Azadmanjiri J. Structural and electromagnetic properties of Ni–Zn ferrites prepared by sol–gel combustion method. *Materials Chemistry and Physics* 2008;**109**:109–12.
5. Zahi S, Daud A, Hashim M. A comparative study of nickel–zinc ferrites by sol–gel route and solid-state reaction. *Materials Chemistry and Physics* 2007;**106**:452–6.
6. Wu K, Ting T, Li M, Ho W. Sol–gel auto-combustion synthesis of SiO_2-doped NiZn ferrite by using various fuels. *Journal of Magnetism and Magnetic Materials* 2006;**298**:25–32.
7. Liu C, Zou B, Rondinone A, Zhang Z. Reverse micelle synthesis and characterization of superparamagnetic $MnFe_2O_4$ spinel ferrite nanocrystallites. *The Journal of Physical Chemistry* 2000;**B104**:1141–5.
8. Komarneni S, D'Arrigo M, Leonelli C, Pellacani C, Katsuki H. Microwave-hydrothermal synthesis of nanophase ferrites. *Journal of the American Ceramic Society* 1998;**81**:3041–4.
9. Búcko M, Haberko K. Hydrothermal synthesis of nickel ferrite powders, their properties and sintering. *Journal of the European Ceramic Society* 2007;**27**:723–7.
10. Hallynck S, Pourroy G, Vilminot S, Jacquart P-M, Autissier D, Vukadinovic N, et al. Synthesis of high aspect ratio of $Ni_{0.5}Zn_{0.5}Fe_2O_4$ platelets for electromagnetic devices. *Solid State Sciences* 2006;**8**:24–30.
11. Yang Z-H, Gong Z-Q, Li H-X, Ma Y-T, Yang Y-F. Synthesis of Ni–Zn ferrite and its microstructure and magnetic properties. *Journal of Central South University of Technology* 2006;**61**:8–623.
12. Rao B, Kumar A, Rao H, Murthy Y, Caltun O, Dumitru I, et al. Synthesis and magnetic studies of Ni–Zn ferrite nanoparticles. *Journal of Optoelectronics and Advanced Materials* 2006;**8**:1703–5.
13. Shenoy S, Joy P, Anantharaman M. Effect of mechanical milling on the structural, magnetic and dielectric properties of co-precipitated ultrafine zinc ferrite. *Journal of Magnetism and Magnetic Materials* 2004;**269**: 217–26.
14. Hsu W-C, Chen S, Kuo P, Lie C, Tsai W. Preparation of NiCuZn ferrite nanoparticles from chemical co-precipitation method and the magnetic properties after sintering. *Materials Science and Engineering* 2004;**B111**:142–9.
15. Costa A, Silva V, Cornejo D, Morelli M, Kiminami R, Gama L. Magnetic and structural properties of $NiFe_2O_4$ ferrite nanopowder doped with Zn^{2+}. *Journal of Magnetism and Magnetic Materials* 2008;**320**:e370–2.
16. Krell A, Blank P, Ma H-W, Hutzler T, Nebelung M. Processing of high-density submicrometer Al_2O_3 for new applications. *Journal of the American Ceramic Society* 2003;**86**:546–53.
17. Yu L, Zhang J, Liu Y, Jing C, Cao S. Fabrication, structure and magnetic properties of nanocrystalline NiZn-ferrite by high-energy milling. *Journal of Magnetism and Magnetic Materials* 2005;**288**:54–9.
18. Bid S, Pradhan S. Characterization of crystalline structure of ball milled nano-Ni–Zn–ferrite by Rietveld method. *Materials Chemistry and Physics* 2004;**84**:291–301.
19. Sepelak V, Schultze D, Krumeich F, Steinike U, Becker K. Mechanically induced cation redistribution in magnesium ferrite and its thermal stability. *Solid State Ionics* 2001;**141–142**:677–82.
20. Ding J, Liu X, Wang J, Shi Y. Ultrafine ferrite particles prepared by co-precipitation/mechanical milling. *Materials Letters* 2000;**44**:19–22.
21. Feick G, Hainer R. A temperature-limiting mechanism in the thermal decomposition of ammonium nitrate. *Nature* 1954;**173**:1188–9.
22. Properties UNIDO and International Fertilizer Development Center. *Fertilizer manual*. Kluwer Academic Publishers; 1998. ISBN 0-7923-5032-4.
23. Costa A, Diniz A, Silva V, Kiminami R, Cornejo D, Gama A, et al. Influence of calcination temperature on the morphology and magnetic properties of Ni–Zn ferrite applied as an electromagnetic energy absorber. *Journal of Alloys and Compounds* 2009;**483**:563–5.
24. Majewski P, Krysinski P. Synthesis, surface modifications, and size-sorting of mixed nickel–zinc ferrite colloidal magnetic nanoparticles. *Chemical European Journal* 2008;**14**:7961–8.
25. Herzer G. Nanocrystalline soft magnetic alloys. In: Buschow KHJ, editor. *Handbook of magnetic materials*, vol. 10; 1997, p. 415–62.
26. Kukolev G, Ya Piven I, Polishchuk V. The effectiveness of wet milling materials in ball mills. *Glass and Ceramics* 1972;**29**(4):251–3.
27. Manova E, Paneva D, Kunev B, Rivière E, Estournès C, Mitov I. Characterization of nanodimensional Ni–Zn ferrite prepared by mechanochemical and thermal methods. *Journal of Physics: Conference Series* 2010;**217**, 012102-1–4.